Western Indian Ocean

JOURNAL OF

Marine Science

Western Indian Ocean
J O U R N A L   O F
Marine Science

Published biannually

Aims and scope: The *Western Indian Ocean Journal of Marine Science* provides an avenue for the wide dissemination of high quality research generated in the Western Indian Ocean (WIO) region, in particular on the sustainable use of coastal and marine resources. This is central to the goal of supporting and promoting sustainable coastal development in the region, as well as contributing to the global base of marine science. The journal publishes original research articles dealing with all aspects of marine science and coastal management. Topics include, but are not limited to: theoretical studies, oceanography, marine biology and ecology, fisheries, recovery and restoration processes, legal and institutional frameworks, and interactions/relationships between humans and the coastal and marine environment. In addition, *Western Indian Ocean Journal of Marine Science* features state-of-the-art review articles and short communications. The journal will, from time to time, consist of special issues on major events or important thematic issues. Submitted articles are subjected to standard peer-review prior to publication.

Manuscript submissions should be preferably made via the African Journals Online (AJOL) submission platform (http://www.ajol.info/index.php/wiojms/about/submissions). Any queries and further editorial correspondence should be sent by e-mail to the Chief Editor, wiojms@fc.ul.pt. Details concerning the preparation and submission of articles can be found in each issue and at http://www.wiomsa.org/wio-journal-of-marine-science/ and AJOL site.

Disclaimer: Statements in the Journal reflect the views of the authors, and not necessarily those of WIOMSA, the editors or publisher.

Satellite-derived bathymetry:
A case study of Mombasa Port Channel
and its approaches, Kenya

Amon Kimeli [1]*, Pascal Thoya [1], Noah Ngisiang'e [1], Harrison Ong'anda [1], Charles Magori [1]

[1] Kenya Marine and Fisheries
Research Institute,
PO Box 81651-80100, Mombasa,
Kenya

* Corresponding author:
kimeli.k.amon@gmail.com

Abstract

Bathymetry refers to the depth of the water column in relation to sea level. It is fundamental in marine spatial planning, resource exploration and sustainable management of marine resources. It is also vital for safety of navigation, and planning of coast-based infrastructural developments. However, acquisition of bathymetry data is very expensive due to the cost of equipment, expertise and technology needed to collect data and produce maps. Satellite-derived bathymetry (SDB) therefore offers an opportunity to generate shallow water bathymetry at extremely reduced costs, mainly due to freely-available multispectral satellite imagery and open-source processing software. This paper presents the application of an already developed and published shallow-water bathymetry derivation model and protocols. The results indicate that the technique could be effective for mapping shallow water bathymetry, with higher accuracy in low to non-turbid waters. The SDB of Mombasa Port was identical to the official charted depths upon comparison, with a R^2 value of ~90% and a RMSE of 1.61 m. SDB maps can be categorized as medium resolution due to their relatively low spatial resolution. SDB cannot be used as a stand-alone hydrographic tool but it rather offers a viable reconnaissance solution for mapping shallow coastal waters where hydrographic data gaps exist.

Keywords: bathymetry, remote sensing, satellite imagery, Landsat 8, models

Introduction

The costs of obtaining high resolution bathymetric data are extremely high. This is attributed to the high cost of equipment (e.g. multibeam and singlebeam echosounders, sidescan sonars, remotely and automatically operated vehicles), platforms (research vessels), specialized processing software, and expertise. Dedicated research vessels and the expertise needed are still inadequate in most developing countries (Pe'eri *et al.*, 2014). Traditionally, bathymetry data was mainly used for updating navigational charts, but it is now gaining prominence in mapping the seafloor for scientific purposes, including for fisheries management, tsunami propagation modelling, and for the oil and gas industry. The need for bathymetry data has also been raised by the heightened focus on the blue economy for the sustainable use of marine resources and development. Therefore, the development of freely-available resources, open source and

cost-effective tools for obtaining bathymetry could improve the capability of developing countries to collect bathymetric data. These tools and resources should be able to assist in assessing geomorphological changes and provide reliable reconnaissance for further directed and detailed surveys.

One of the emerging tools for establishing bathymetry is the derivation of bathymetry from multispectral satellite imagery. Satellite-derived bathymetry (SDB) is a survey method founded on empirical and analytical modelling of light penetration through the water column in visible bands of multispectral satellites (Pacheco *et al.*, 2015; Laporte *et al.*, 2014; Pe'eri *et al.*, 2014; Lee *et al.*, 1999; Philpot, 1989; Lyzenga, 1985). Major advantages of these methods are the availability of freely-available satellite data (e.g. Landsat and Sentinel), new sensors with added capabilities, open source processing software (e.g. QGIS)

and scientific literature and case studies (Barber *et al.*, 2016). SDB has been gaining acceptance in recent years (Pacheco *et al.* 2015; Pe'eri *et al.* 2014; Bramante *et al.*, 2013; Stumpf *et al.*, 2003; Lyzenga, 1985). Despite the developments over time, SDB still offers low resolution maps compared to some traditionally accepted acoustic surveying techniques such as multibeam surveys (MBES) which offer full sea-floor coverage of up to 0.5 m resolution (IHO, 2008). According to Barber *et al.* (2016), this accuracy can be attributed to the large spatial resolution of available satellite platforms (2 m for sentinel-2, and 15 – 30 m for Landsat 8). However, SDB could offer better resolutions than point-based methods including lead-lines and singlebeam (SBES) echosounders where data points could vary in the spatial scale. Although there has been gradual development of SDB methodology, published information has always concentrated on algorithm and model development, and it is only very recently that case studies have been conducted. This paper utilizes the water radiances of three bands of Landsat 8 (infrared 1560-1660 nm; green: 525-600 nm; blue: 450 – 515 nm) to retrieve and estimate shallow water bathymetry. Landsat 8 carries two sensors (the Operational Land Imager (OLI) and the Thermal Infrared Sensors (TIRS)) with eleven bands of various capabilities (Irons *et al.*, 2012). A typical multispectral satellite sensor has several channels individually capturing a broad (70 -150 nm) spectral range (Pe'eri *et al.*, 2014). They also collectively cover the entire electromagnetic spectrum (visible to infrared) ranging between 433 – 1390 nm. The fundamental concept that underpins SDB is the exponential wavelength-dependent light transmittance, penetration and attenuation in water with respect to depth (Laporte *et al.* 2015; Pacheco *et al.*, 2014; Pe'eri *et al.*, 2014). According to Pe'eri *et al.*, 2014 (originally in Jerlov, 1976), 350 nm (ultra-violet) – 700 nm (red) represents the range of wavelengths of light that are less attenuated in seawater for relatively considerable depths. However, wavelengths greater than 700 nm (near infrared) are attenuated easily in seawater and are therefore suitable for delineating the land and seawater boundary. It is therefore from the visible bands (red, green and blue) between 450 – 690 nm, that the principle of estimation of depth is anchored. In order to derive bathymetry estimates, existing bathymetric data (e.g. chart soundings, LiDAR) should be used to vertically reference the SDB and convert the SDB raster image to depth. The Lowest Astronomical Tide (L.A.T in metres) tidal datum used in this study is the official Kenyan chart

datum for all nautical/navigation charts. For optimal use of the SDB method, several other environmental requirements that could affect the estimation of bathymetry and introduce errors need to be considered. These include water clarity, satellite images without and/or with minimal sun glint, and cloud and optically active materials in the water column such as suspended matter and aquatic vegetation.

Several models and algorithms have been developed over time for SDB (Pe'eri *et al.*, 2014; Stumpf *et al.*, 2003; Lyzenga, 1985; Lyzenga, 1978). The models, according to Pe'eri *et al.* (2014), can be categorized into three broad categories: i) analytical models that utilizes radiative transfer models for specific data (Lyzenga, 1978; Philpot, 1989); ii) comparative models that utilize large datasets generated from radiative transfer models (Bramante *et al.*, 2013; Louchard *et al.*, 2003); and finally iii) the optimization band ratio model used in this paper, based on the assumption of vertically-invariant water column and seabed condition (Pe'eri *et al.*, 2014; Stumpf *et al.*, 2003). The three models are mathematically hinged on the exponential decay of radiance (W m^{-2} sr^{-1} nm^{-1}) with water depth (Mobley, 2004). According to Philpot (1989), the observed radiance in shallow water can be represented as shown in the equation below:

$$L_{obs} = (L_b - L_{w)} \cdot e^{-2k(\lambda),z} + L_w$$

Where L_{obs} is the observed radiance, L_b is the radiance contribution from the sea bottom, L_w is the observed radiance over optically deep waters, z is the water depth (m), and $k(\lambda)$ is the diffuse attenuation coefficient (Bramante *et al.*, 2013; Mobley, 2004). Therefore, the equations $L_{obs} = L_b$ (at Z=0) and $L_{obs}=L_b$ (Z=∞) holds.

The general assumption for the optimization band ratio model is that the sea bottom is homogenous and therefore the reflectance and attenuation is uniform. In reality though, shallow coastal areas are among the most dynamic in terms of wave and sediment dynamics. According to Pe'eri *et al.* (2014), the utilization of ratio transform in this approach yields robust bathymetry without necessarily sampling the dynamic environment.

For vertical referencing purposes, official Kenyan navigational charts were used. The official navigation chart for Mombasa and its approaches is based on diverse data from lead line (as old as 1880s), single-beam data, and multibeam surveys. Kenya's official

charting agency is the United Kingdom Hydrographic Office (UKHO), and they produce official charts for Kenya under the British Admiralty (BA). The area covering the port of Mombasa and its approaches is covered by the navigational chart BA666. A 30th May 2015 Edition 3 chart with a scale 1:12500 was used. The objective of this study was therefore to apply the optimization band ratio model to retrieve shallow water bathymetry for the Mombasa Port Channel and its approaches, and compare with officially charted depths.

Study Area

The coastal waters in and around Mombasa port and its environs (Fig. 1) were chosen as the site for the derivation of bathymetry from satellite imagery because of its importance to Kenya's maritime trade. The other reason was the availability of a high-resolution navigational chart for the area for referencing the SDB. The climate in Kenya is monsoon-influenced and there are two distinct seasons, namely the rainy and the dry seasons. The southeast monsoon (SEM) between April and July is characterized by long rains while the northeast monsoon (NEM) between October

and November is characterized by short rains with a mean annual precipitation of 1144 mm (Verheyden *et al.*, 2005, originally in Lieth *et al.*, 1999). The Kilindini channel which hosts the Mombasa Port harbor is tide dominant but also receives seasonal inflow from the Mwache River during rainy seasons. Hydrodynamically, it is characterized by semi-diurnal tides with tide amplitudes of up to 3m with respect to the lowest astronomical tide (L.A.T).

Materials and Methods

In this paper, freely-available Landsat 8 satellite imagery were used because they were easy to obtain and readily available. Additionally, their 185 km swath coverage allows for processing images that cover larger areas; for example, only two images cover the entire Kenyan coast. The optimization model using band ratio calculation according to Pe'eri *et al.* (2014), Philpot *et al.* (2004), and Stumpf *et al.* (2003) was used to derive the shallow bathymetry as described in the introduction. Subsurface reflectance was transformed to spectral reflectance based on analytical equations for irradiance reflectance (W m^{-2} nm^{-1}), and remote-sensing reflectance according to Pacheco *et al.*
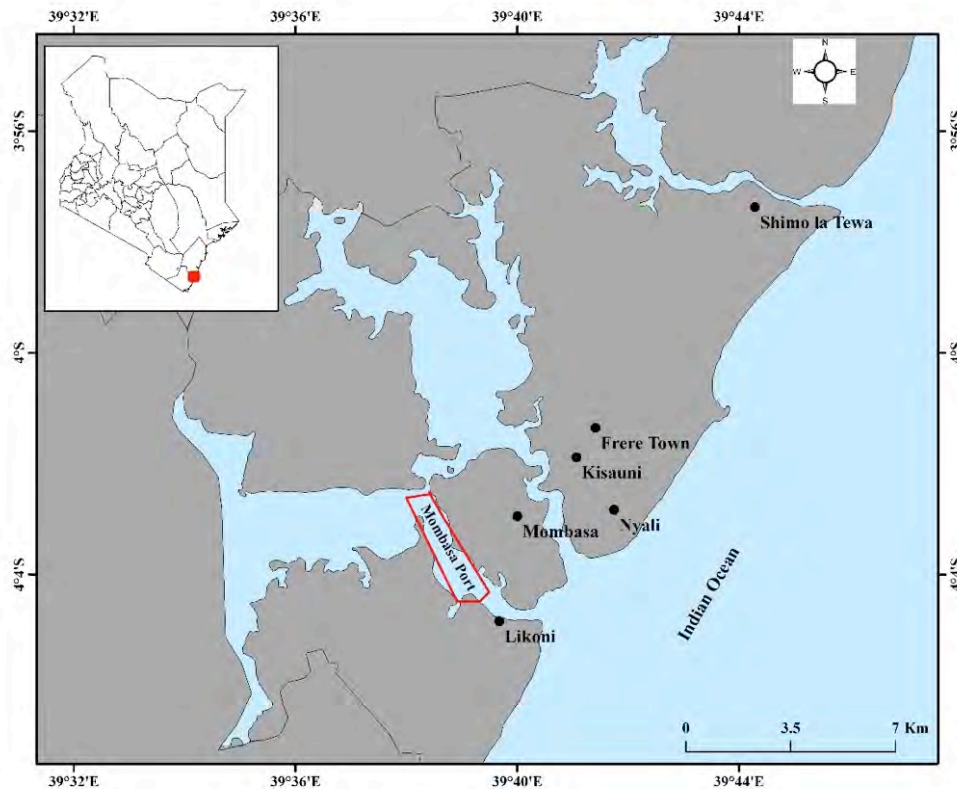

Figure 1. Mombasa Port channel and its approaches with the two distinct creeks, i.e. the southern Mwache Creek (Kilindini main channel of Mombasa Port), and northern Tudor Creek.
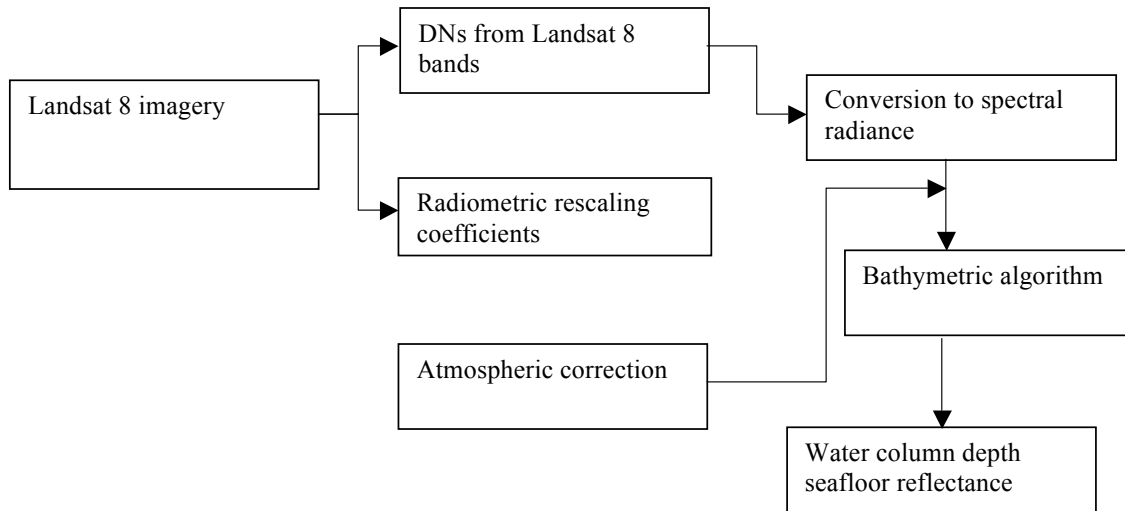
Figure 2. Workflow for deriving SDB maps from Landsat 8 images. This workflow is compatible with most accessible satellite data. (Modified from Pacheco et al., 2014).

(2014). The process of deriving bathymetry follows well-defined procedures from data (image) acquisition to referencing, as shown in the schematic workflow (Fig. 2).

Image Acquisition

Standard bulk Landsat 8 satellite images (band 1 to band 11) were downloaded from http://earthexplorer.usgs.gov/. Bands 1 to 7, and 9, have a spatial resolution of 30 m, while band 8 has a spatial resolution of 15 m, and bands 10 and 11 has a spatial resolution of 100 m (Pacheco *et al.*, 2014). Additionally, the standard bulk download of Landsat 8 imagery has an extra metadata file (MTL file) containing the radiometric Top of Atmosphere (TOA) rescaling coefficient, and this was also acquired. Satellite scenes from April 10, 2015 were downloaded considering earlier mentioned parameters (i.e. cloud free image and minimal sun glint). The satellite scenes downloaded covered the Kenyan south coast from Vanga to Kilifi, inclusive of the port
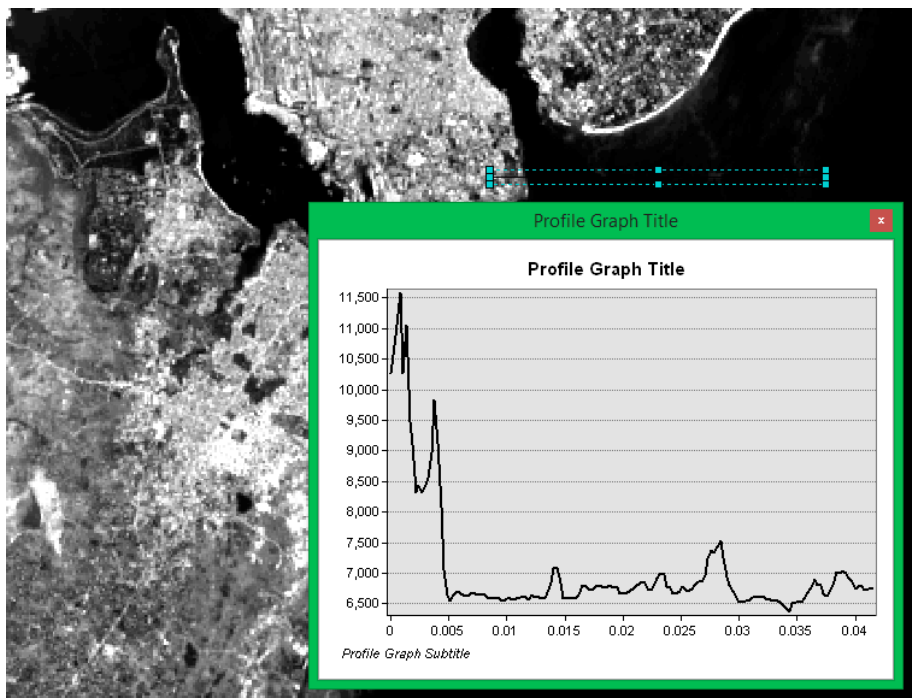

Figure 3. Land-Sea profile from a profile in NIR band with high (>6500-pixel) values corresponding to land and the low (<6500-pixel) values in the y-axis.

of Mombasa (Kilindini Harbour). The downloaded images were georeferenced to the WGS84 datum and projected to UTM zone 37S.

Preprocessing

A threshold depicting the transition between the land and water was defined by a combination of "identify" tool and the "profile" function in ArcMap toolbox. The profile method shows spiky sections representing land, and much smoother sections depicting water bodies (Fig. 3). The point of transition between the two regions signifies the threshold/cutoff value between land and water (Fig. 4). Additionally, the identify tool examines the pixel values both on land (high values) and water (low values), and since the water is close to opaque, it appears dark in the near-infrared (NIR), and bright on land due to reflection. From the selected values a threshold can be inferred from the transition between the low (water values) to high (land) pixel values. A low pass filter was applied to remove inherent radiometric noise in the imagery caused by "radiometric mal-adjustments" (Pe'eri *et al.*, 2013; Gao *et al.*, 2000) and brightness in the image (sun glint). Since the study site is situated in the tropics and is characterized by increased cloud coverage, cloud filtering was also performed as described in Pe'eri *et al.* (2014). Land, water and clouds are reflected well in near infrared (NIR), subsequently the histogram of the NIR band over a coastal area is bimodal, meaning the histogram will have two peaks; one corresponding to land and the other water. Furthermore, remaining

cloud shadows and sun glint after masking and separation were removed using the Hedley *et al.* (2005) approach expressed in the equation below:

$$L'_{obs}(\lambda_i) = \left((L_{obs}(\lambda_i)) - b_i \cdot \left((L_{obs}(NIR)) - Min(L_{obs}(NIR))\right)\right)$$

Where the pixel value in band i, $L_{obs}(\lambda_i)$ is a reduced by-product of the regression slope, b_i, and the difference between the pixel NIR value, $L_{obs}(NIR)$, and the ambient NIR level, $(Min(L_{obs}(NIR))$.

Deriving estimated bathymetry

The optimization band ratio model as described in Pe'eri *et al.* (2014) was then applied on the filtered images to estimate bathymetry by the ratios of blue and green bands. Specifically, the Stumpf *et al.* (2003) and Dierssen *et al.* (2003) log ratio model, which is a sub-category of the optimization band ratio model, was used. Based on the earlier described assumption of water column homogeneity, the difference of attenuation coefficient values (band ratio) will have a near-constant attenuation value. The use of two bands significantly reduces the number of parameters that would be required to compute the bathymetry (Stumpf *et al.*, 2003). Therefore, the variation in ratio between the bands with respect to depth can be deduced. In non-turbid shallow coastal waters, the light in the blue wavelengths attenuates faster than the light in the green wavelengths (Jerlov, 1976), and based on the fact that the two bands experience similar decay behavior, the model reduces errors associated with spectral reflectance in atmosphere,
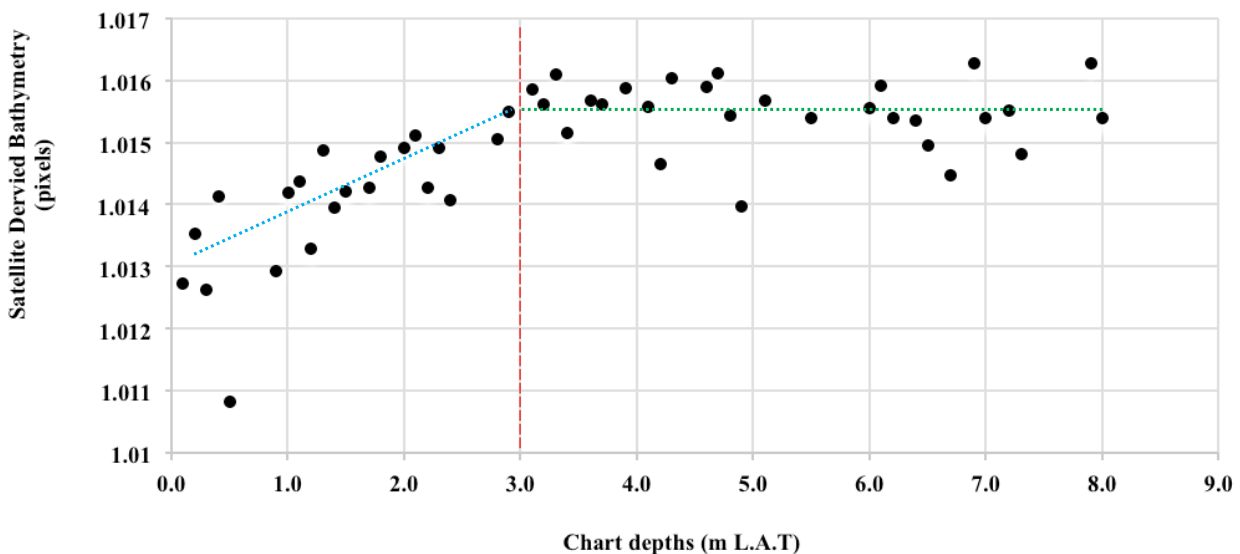

Figure 4. Scatter plot of chart depths and SDB (raster values) for the identification of the extinction depth (red dotted vertical line). In this case the ED is 3 m with visible inflection of curve from diagonal (blue dotted line) to horizontal (green dotted line).
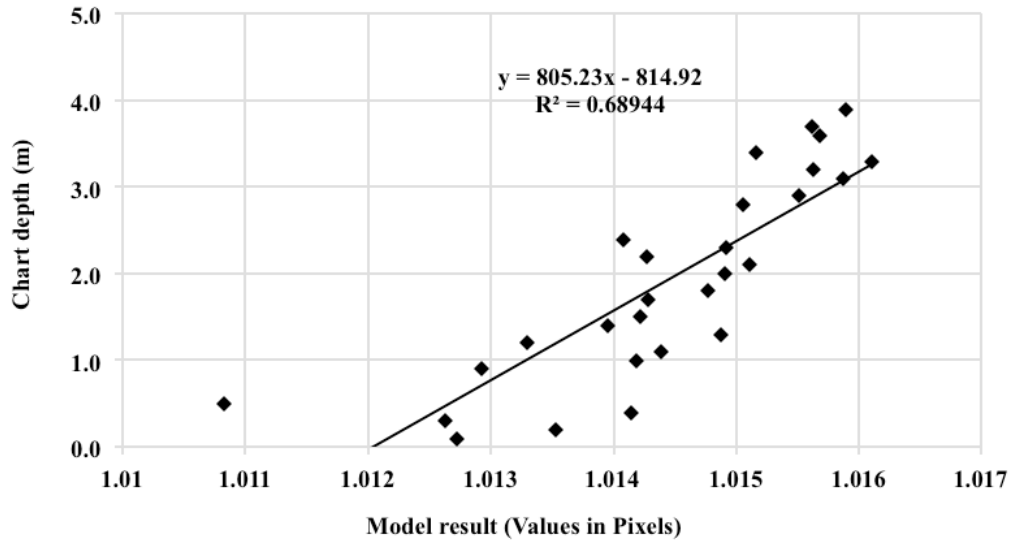
Figure 5. Regression analysis determining the gain and offsets for vertical referencing.

water column and sea bottom. The optimization band ratio model then estimates depth using reflectance of each spectral band, calculated with sensor calibration files and atmospheric artifacts corrected.

The optimization band ratio model is represented by the equation below;

$$Z = M_1 \left(\frac{\ln (nR_w(\lambda_1))}{\ln (nR_w(\lambda_2))} \right) - M_0$$

Where $R_W(\lambda_1)$ and $R_W(\lambda_2)$ are the pixel values corresponding to two reflectance bands λ_1 and λ_2 respectively. M_1 and M_0 are the gains and offset used to convert the algorithm result to depth relative to navigational chart datum. The value n is used to ensure that the logarithmic result is positive at all times, and the ratio subsequently produces a linear response.

Correlating the Landsat images with published chart soundings allowed for the determination of extinction depths, or the depth where bottom reflections affect the pixel values (typically in shallow waters). According to Pe'eri et al. (2014), only two points are adequate to determine the extinction depth, but several points are recommended for redundancy purposes (i.e. determination of "statistically optimal values of gain and offset"). Areas deeper than the extinction depth (equivalent to 2 secchi disk depths) are represented by value of water depth. The standard bathymetry algorithm has a theoretical derivation (Stumpf *et al.*, 2003; Dierssen *et al.*, 2003; Lyzenga, 1978), but also incorporates empirical tuning as an inherent part of the depth estimation process. According to available literature (Pacheco *et al.*, 2014; Lyzenga, 1985), it is preferable to

minimize such tuning, particularly for remote regions where benthic and water quality parameters can be difficult to measure or estimate.

Referencing to a vertical datum
The algorithm results are referenced to a chart datum and it has been proven that shallower areas show linear correlation as opposed to the deep waters (Pe'eri *et al.*, 2014). This process also assists in checking the adequacy of navigational charts. The aforementioned linearity, or lack of it, can be determined by examining the regression coefficient (R^2) with values close to 1, signifying high correlation (Fig. 5).

Results
Vertical referencing and determination of extinction depth
This step required the determination of gain and offsets to be used in referencing the algorithm- derived bathymetry to the chart datum (see Pacheco *et al.*, 2014; Pe'eri *et al.*, 2014). The graph (Fig. 4) shows a gradual linear line at shallow depth that starts to curve and flatten out horizontally in deeper water. The exact point of inflection represents the extinction depth, which in this case was determined to be approximately 3 m (Fig. 4). However, this value could vary depending on the region and the variation can be attributed to variability in cloud cover and turbidity with time and area of interest. Variability could also arise from the fact that the extinction is based on the visual observation of the graph which varies from one person to another. From the scatter plot of chart depths obtained from digitizing the navigation chart (BA666) versus the raster values (Fig. 5), the slope (gain) and y-intercept (offset) values required
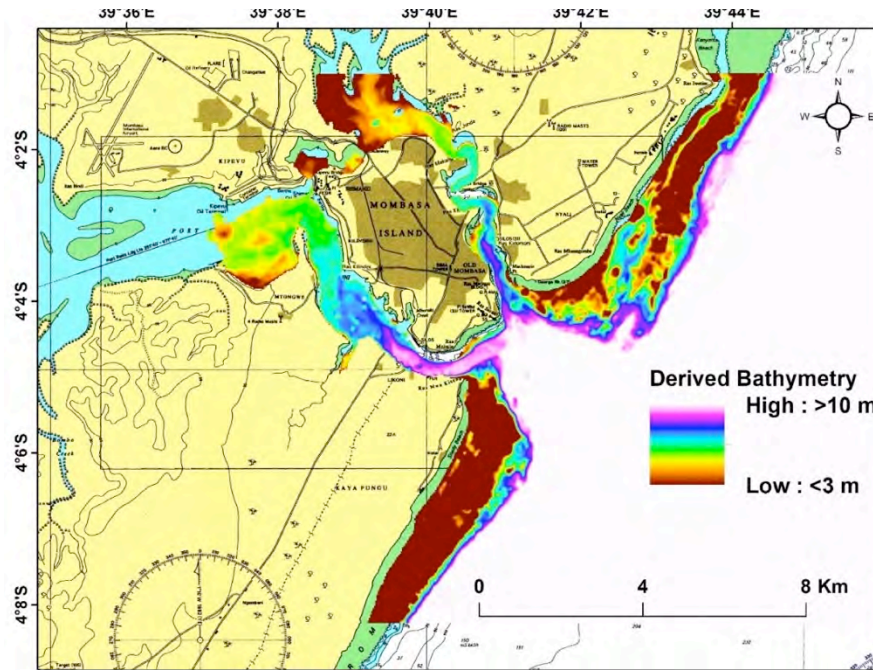
Figure 6. Derived shallow water bathymetry of Mombasa Port and its approaches.

for vertically referencing the SDB to chart datum were recorded as 805.23 and -814.92 respectively.

Derived bathymetry

The referenced SDB of Mombasa Port and its approaches is represented in Fig. 6. The depths generated showed a variation from as shallow as 5 m to depths greater than 10 m. This specific part of navigable areas of the sea present the highest risks to shipping, such as grounding. Selected charted depths and SDB showed great similarity (Fig. 7). For example, a charted depth of 2.2 m corresponded to a derived depth of 2.25 m. Furthermore, a linear regression analysis of the chart depth and the derived depths was
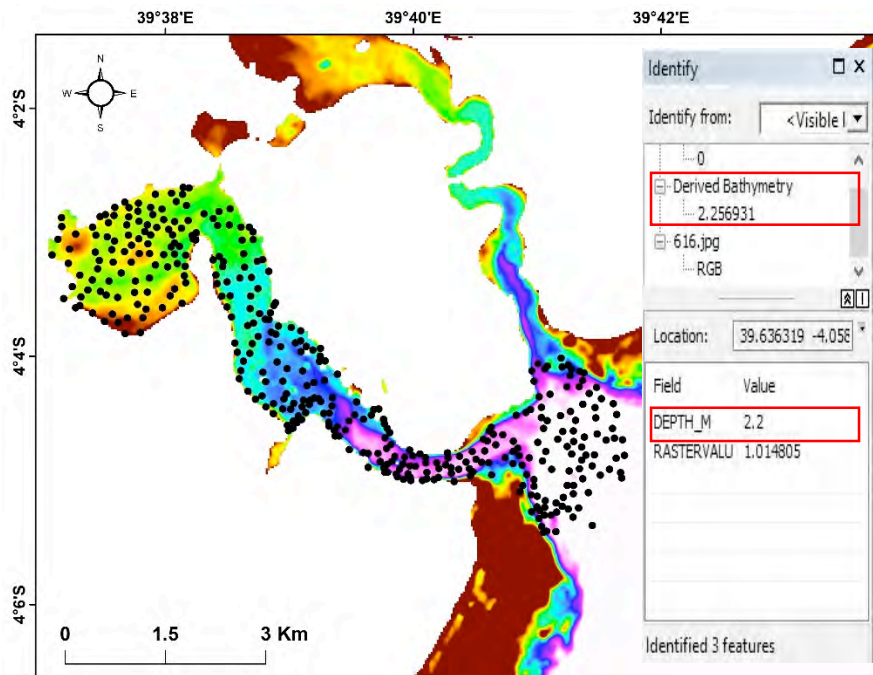

Figure 7. Comparison of derived bathymetry and the chart depths of Mombasa Port and its approaches. Inset is the identify tool in ArcMap showing the values of all visible layers; in this case the digitized water depth (black dots) and the derived depths.
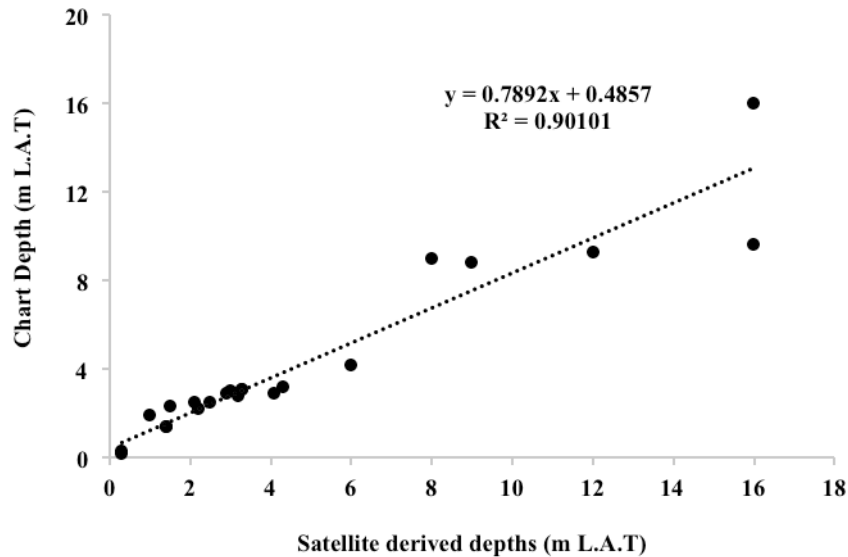
Figure 8. Regression graph of the chart depths (m L.A.T) vs derived depths (m L.A.T).

performed, and there was good linearity of the SDB versus the charted depths (Fig. 8), with a R^2 value of 0.90 and a root mean square error (RMSE) of 1.61 m.

Discussion

An excellent correlation between SDB and charted depths (R^2 =~90%) was obtained re-affirming the strength of analytical models in estimating bathymetry from satellite imagery. The results from this study are also similar to other previous studies (Jagalingam *et al*., 2015; Pacheco *et al*., 2015; Brando *et al*., 2009). It is also worth noting that, except for Jagalingam *et al.* (2015), all the other studies did not use charted soundings to vertically reference their derived bathymetry. Pacheco *et al*. (2015) and Pe'eri *et al*. (2014) utilized airborne laser bathymetric (ALB) light detection and ranging (LiDAR). This shows that the band ratio model of retrieving bathymetry can be reproduced in a wide range of diverse environmental setting and at different times. Barber *et al.* (2016) used satellite imagery from different months and different locations and found that there was a good correlation (-/+ 1 m standard deviation). They also noted that even in remote areas, with favorable environmental conditions, bathymetry could still be retrieved. However, the main limitations of SDB is the reliance on good environmental conditions including water clarity (turbidity), depth, wave dynamics and meteorological conditions (e.g. presence/absence of clouds). To overcome some of these challenges, better estimation of bathymetry could be achieved by incorporating corrections for variables that could affect the estimation of bathymetry in the models. Some of the environmental variables that

could cause errors in estimated bathymetry include the presence of optically active constituents in the water column (Pacheco *et al*., 2015). These variables include chlorophyll-a, dissolved organic matter and particulate matter. SDB is suitable for calm waters with minimal turbulence because turbulence creates bubbles that are also optically active. These factors subsequently affect the derivation and accuracy of bathymetry (Laporte *et al.*, 2015; Pe'eri *et al.*, 2014; Louchard *et al.*, 2003; Lee *et al*., 1999; Sandidge and Holver, 1989). For example, the low R^2 value observed could be attributed to a low-resolution hydrographic chart (Jagalingam *et al*., 2015) and updates are recommended. Knowledge of these conditions, including their temporal and spatial occurrences, assists in a better understanding of bathymetry to be generated. SDB is modeled from light penetration and attenuation of variation in different spectral bands in water. Light penetration, attenuation and reflectance are inhibited and/or affected by the presence of suspended organic and inorganic materials. The depth of the seafloor can only be estimated to the extent of light penetration, and since turbidity will also lead to a "false shoaling" (Pe'eri *et al*., 2014) incorrect bathymetry can be recorded. Suspended particles will therefore give a false reflection and jeopardize the accuracy of the generated bathymetry. Additionally, according to Lee *et al*. (1999), this technique avails itself to rapid data processing. However, it requires knowledge of a "few true depths for the regression parameters to be determined, and it cannot reveal in-water constituents". Therefore, the SDB described in this paper offers, among other benefits, a good coverage within

depth and image limitations, and better depth resolution than traditional point-based methods such as lead line and singlebeam (SBES) acoustics.

Conclusion

From the statistics it can be concluded that the optimization band ratio model can retrieve depths in shallow waters. SDB offers a viable reconnaissance solution for areas of shallow coastal water where there is little or no existing hydrographic data, and no prospect of obtaining the resources required to proceed with extensive surveys using other higher accuracy methods in the foreseeable future. It is therefore a means of gaining information on bathymetry and reconnaissance where full-scale bathymetric mapping (by acoustic/sonar systems) cannot be carried out at a particular moment. It cannot therefore be used as a stand-alone hydrographic surveying tool, but rather as a support technique for hydrographic mapping of particular areas of interest.

Acknowledgements

References

Barber J, Pe'eri S, Klemm A, Nyberg J, Powell J (2016) Sensor-derived policy and localized chart updates at NOAA's Marine Chart Division. Canadian Hydrographic Conference 2016, Halifax, NS, Canada, 16-19 May

Bramante JF, Raju DK, Sin TM (2013) Multispectral derivation of bathymetry in Singapore's shallow, turbid waters. International Journal of Remote Sensing 34 (6): 2070–2088

Brando V, Anstee JM, Wettle M, Dekker AG, Phinn SR, Roelsema C (2009) A physical based retrieval and quality assessment of bathymetry from suboptimal hyperspectral data. Remote Sensing of Environment 113: 755–790

Dierssen HM, Zimmerman RC, Leathers RA, Downes TV, Davis CO (2003) Ocean color remote sensing of seagrass and bathymetry in the Bahamas Banks by high-resolution airborne imagery. Limnology and Oceanography Methods 48: 444-455

Gao BC, Montes MJ, Ahmad Z, Davis CO (2000) An atmospheric correction algorithm for hyperspectral remote sensing of ocean color from space. Applied Optics 39 (6): 887-896

Hedley JD, Harborne RA, Mumby PJ (2005) Technical note: Simple and robust removal of sun glint for mapping shallow-water benthos. International Journal of Remote Sensing 26 (10): 2107-2112

International Hydrographic Organization, IHO (2008) International hydrographic organization standards S-44 for hydrographic surveys. Special publication no. 44. 28 pp

Irons JR, Dwyer JL, Barsi JA (2012) The next Landsat satellite: The Landsat data continuity mission. Remote Sensing of Environment 122: 11-21

Jagalingam P, Akshaya BJ, Hegde VA (2015) Bathymetry mapping using Landsat 8 satellite imagery. Procedia Engineering 116: 560-566

Jerlov NG (1976) Marine Optics. Elsevier Scientific, New York, Vol 14. 231 pp

Laporte J, Hedley J, Mouscardes P (2015) Satellite Derived Bathymetry migration from laboratories to chart production routine. Hydro International 19 (7): 16-19

Lee ZP, Carder KL, Mobley CD, Steward RG, Patch JS (1999) Hyperspectral remote sensing for shallow waters: 2. Deriving bottom depths and water properties by optimization. Applied Optics 38 (18): 3831-3843

Lieth H, Berlekamp J, Fuest S, Riediger S (1999) Climate diagrams of the world. CD-series: climate and biosphere. Blackhuys Publishers, Leiden, the Netherlands

Louchard EM, Reid RP, Stephens CF, Davis CO, Leathers RA, Downes TV (2003) Optical remote sensing of benthic habitats and bathymetry in coastal environments at Lee Stocking Island, Bahamas: a stochastic spectral classification approach. Limnological Oceanography 48 (1): 511-521

Lyzenga DR (1978) Passive remote sensing techniques for mapping water depth and bottom features. Applied Optics 17: 379-383

Lyzenga DR (1985) Shallow-water bathymetry using combined LiDAR and passive multispectral scanner data. International Journal of Remote Sensing 6: 115-125

Mobley CD (2004) Light and water: radiative transfer in neutral waters [CD Rom]. Academic Press, San Diego, CA

Pacheco A, Horta J, Loureiro C, Ferreira Ó (2014) Retrieval of nearshore bathymetry from Landsat 8 images: A tool for coastal monitoring in shallow waters. Remote Sensing of Environment 159: 102-116 [http://dx.doi.org/10.1016/j.rse.2014.12.004]

Pe'eri S, Parrish C, Azuike C, Alexander L, Armstrong A (2014) Satellite remote sensing as a reconnaissance tool for assessing nautical chart adequacy and completeness. Marine Geodesy 37 (3): 293-314

Philpot W, Davis CO, Bissett WP, Mobley CM, Kohler DDR, Lee Z, Bowles J, Steward RG, Agrawal Y, Trowbridge J, Gould Jr RW, Arnone RA (2004) Bottom characterization from hyperspectral image data. Oceanography 17 (2): 76-85

Philpot WD (1989) Bathymetric mapping with passive multispectral imagery. Applied Optics 28 (8): 1569-1578

Sandidge JC, Holver RJ (1998) Coastal bathymetry from hyperspectral observations of water radiance. Remote Sensing of Environment 65: 341-352

Stumpf RP, Holderied K, Sinclair M (2003) Determination of water depth with high-resolution satellite imagery over variable bottom types. Limnology and Oceanography 48: 547-556

Verheyden A, De Ridder F, Schmitz N, Beeckman H, Koedam N (2005) High-resolution time series of vessel density in Kenyan mangrove trees reveal a link with climate. New Phytologist 167 (2): 425-435